Chemical Engineering Journal 393 (2020) 124734

Contents lists available at ScienceDirect

Chemical Engineering Journal

journal homepage: www.elsevier.com/locate/cej

Roles of oxygen and Mn (IV) oxide in abiotic formation of humic substances by oxidative polymerization of polyphenol and amino acid

Jianmei Zou[a,b], Jianzhi Huang[b], Dongbei Yue[a,*], Huichun Zhang[b,*]

[a] School of Environment, Tsinghua University, Beijing 100084, China
[b] Department of Civil Engineering, Case Western Reserve University, Cleveland, OH 44106, United States

HIGHLIGHTS

- First comprehensive study of the individual roles of MnO_2 and O_2 in humification.
- O_2 was a major oxidant in the accumulation of humification product.
- The main role of MnO_2 was a catalyst during the humification process.
- The direct oxidation by MnO_2 was only limited to the transformation of FA.

GRAPHICAL ABSTRACT

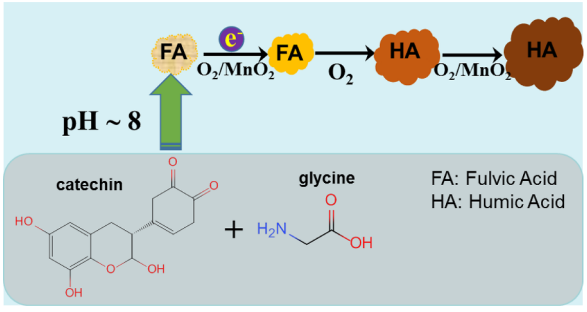

ARTICLE INFO

Keywords:
Catechin
MnO_2
Humification
Fulvic acid
Humic acid
Polyphenols

ABSTRACT

The metal oxide-facilitated transformation of polyphenols and amino acids to humic substances (HS) is an essential process in soil and compost maturing processes. The objective of this research was to examine the specific roles of MnO_2 and O_2 in the formation of HS by oxidative polymerization of catechin (a polyphenol) and glycine (an amino acid). The results demonstrated that large amounts of fulvic acid (FA) and humic acid (HA) only formed in the presence of O_2, while the presence of both O_2 and MnO_2 significantly enhanced HA formation, demonstrating their synergistic effects. The size of HA only increased in the presence of MnO_2, but MnO_2 without O_2 was unable to convert FA to HA. Two-dimensional correlation spectroscopy results suggested that the sequence of the formation of HA functional groups was: C–OH in carboxylic acids > C–O in phenolic-OH > amide II and aromatic C–C > amide and carboxylate C=O > COO^- > NH > hydrogen bond. Finally, XPS spectra of the MnO_2 before and after the reaction showed that the Mn(IV) content decreased from > 99% to 89.98% and 80.89% while the Mn(III) content increased from < 0.1% to 10.02% and 15.07% during the humification in the presence of MnO_2 with and without O_2, respectively, suggesting that the role of MnO_2 was mostly a catalyst but was also an oxidant. These results offered new insights into the abiotic humification process and can help develop efficient treatment technologies for bio-wastes.

1. Introduction

Humification is one of the least understood but most intriguing aspects of humus chemistry [1], during which the formation of humic substances (HS), including humic acids (HA) and fulvic acids (FA), is a complex transformation process. In addition to being crucial in the formation of ubiquitous natural organic matter, humification is a key process in composting, an economical and environmentally friendly

* Corresponding authors.
E-mail addresses: yuedb@tsinghua.edu.cn (D. Yue), hjz13@case.edu (H. Zhang).

https://doi.org/10.1016/j.cej.2020.124734
Received 14 January 2020; Received in revised form 29 February 2020; Accepted 9 March 2020
Available online 10 March 2020
1385-8947/

process to treat organic matter in bio-wastes [2,3]. Stabilized compost products can be applied to soil as organic fertilizers to improve soil properties and promote plant growth, which is of considerable importance in reducing carbon emission and improving land use [4,5]. Because the degree of humification has been commonly used as an indicator for compost maturity during composting [6–9], a better understanding of the humification process will help obtain high quality, mature compost products as well as reduce greenhouse gas emission.

Since the seminar work by Shindo and Huang on the pivotal role of Mn(IV) oxides in abiotic humification [10,11], numerous follow-up research has investigated the oxidative polymerization of simple polyphenols and a representative amino acid (glycine) under a wide range of conditions, including different polyphenols (e. g., catechol, hydroquinone, pyrogallol, and resorcinol), different metal oxides (Al, Fe, Mn, or Si oxides) or clay minerals, temperature and pH [12–16]. In particular, owing to the relatively high reduction potentials and mixed valence configurations, Mn(IV) oxides were reported to have better promoting effects than other metal oxides, with the reactivity in the sequence of Mn oxide $\gg$ Fe oxide $>$ Al oxide $\approx$ Si oxide. Mn(IV) oxides were believed to first promote the ring cleavage of polyphenols [17,18], facilitate the deamination of amino acids, and then accelerate the polycondensation of these compounds to form HS. The polyphenols acted as the backbone and underwent coupling reactions to initiate the oxidative binding of the phenols or amino acids [14,19,20]. Therefore, the induced HS formation in the abiotic humification of polyphenol-amino compounds seems to be a reasonable mechanism for the humification process.

Most of the previous studies on the abiotic humification were conducted in closed systems containing a small amount of O_2, which made the individual roles of the metal oxides and O_2 in the process still ambiguous [11,12,21,22]. Two studies have attempted to examine how O_2 and metal oxides were involved in the oxidation of polyphenols (without amino acids) under either air or N_2 conditions. In one study, Wang and Huang (2000) found that O_2 and metal oxides had synergistic effects in promoting the transformation of pyrogallol [15]; in another study, similar results were obtained on the oxidative polycondensation of three simple polyphenols [23]. These two related research indirectly speculated that O_2 acted as an oxidant and the speculation was only based on monitoring the amounts of CO_2 released during the reaction. Also, the role of MnO_2 remained unidentified. Note that MnO_2 has been demonstrated as promising catalysts [24] or oxidants that might have been involved in both direct and catalytic oxidation [25,26] in a diverse range of chemical reactions in environmental remediation. However, although previous papers on abiotic humification mostly claimed the manganese oxides as catalysts, the mechanisms reported were in fact direct oxidation, as shown in Eq. (1) [10,11,15]. Therefore, it is of great importance to investigate the specific roles of manganese oxides and O_2 in these processes.

$$MnO_2 + 4H^+ + 2e^- \rightarrow Mn^{2+} + 2H_2O \quad (1)$$

In addition, the literature on the evolution of abiotic humification products only monitored the formation of HS by measuring either the time course of the supernatant using UV–vis or the production ratio of HS after isolation. When it comes to characterizing the formed HS, almost all research just examined the end products, although with many different analytical tools such as FTIR and NMR, whereas the evolution of both the product sizes and the characteristic structures of HS has received little attention.

The aim of this work was to elucidate the respective roles of manganese oxides and O_2 on the transformation of polyphenol-amino compounds to HS and to obtain the time course of the stable humification product, i.e., HA. To achieve this goal, we examined the reaction between catechin and glycine in four systems: 1) with MnO_2 under air, 2) without MnO_2 under air, 3) with MnO_2 under N_2, and 4) without MnO_2 under N_2 conditions, which will be referred to as MnO_2 (Air), MnO_2 (N_2), Air, and N_2, respectively. Catechin, a monomer that accounts for around 50–80% of plant polyphenols [27], was selected as a representative polyphenol because most previous studies on abiotic humification only employed simple polyphenols as the model precursors [21,22], which were not able to represent characteristic phenolic compounds in composting. To better compare with previous work, glycine was still employed as the representative amino acid. The extinction coefficient E600 was used to evaluate the degree of humification [21,22,28,29]. HS was also extracted at different incubation times to examine the time courses of the HS production in the four systems in terms of both quantity and quality. The abundance (%) of FA and HA in the four systems during the reaction period was analyzed as the DOC concentration. Dynamic light scattering (DLS) was employed to determine the sizes of the formed HA at different incubation times. Furthermore, two-dimensional correlation spectroscopy (2D-COS) FTIR was used to evaluate the temporal sequence of the functional groups during the formation of HS. Finally, the surface Mn valence changes before and after the reactions were obtained through XPS spectra to further identify the role of MnO_2 in the abiotic humification. Overall, this work offered new insights into the abiotic humification process. The findings will improve our understanding of the individual roles of MnO_2 and O_2 in transforming polyphenol-amino acids into HS, which will provide a guidance for better compost treatment and improve carbon sequestration technologies.

2. Materials and methods

2.1. Chemicals and materials

The analytical grade catechin (C) and glycine (G) were obtained from Sigma–Aldrich in China. MnO_2 was purchased from the Sinopharm group of China with the reagent purity grade of $>$ 99%. Based on the XRD spectrum (Fig. S1), we can identify that the crystal structure of the MnO_2 was likely a γ-MnO_2 [5,30].

2.2. Incubation experiments

Sterile conditions were maintained throughout the experiments to ensure that abiotic transformation dominated. All glassware, phosphate buffer, and other apparatus were autoclaved prior to use. Two grams of MnO_2 were suspended by ultrasonification at 100 W for 3 min in a 200-mL aliquot of autoclaved phosphate buffer (0.2 M, pH = 8) containing 0.02% (w/v) thimerosal (an antiseptic agent) in 500-mL 3-neck round-bottom flasks. The molar concentrations of catechin and glycine in all reactions were 0.008 and 0.02 M, respectively, as recommended for the polyphenol-Maillard reaction in previous studies [31,32]. Each flask was previously flushed with N_2 (99.99% purity) to sweep the gases, and was shaken slowly to mix the precursors with MnO_2 and then tightly sealed by a rubber stopper with a condenser-west tube. The reactors were then placed in a water bath at 45 °C [33] and constantly incubated under 100 mL/min of purified air or N_2 stream for a period of 90 h. The motor stirrers with Teflon stirring rods (300 rpm) were inserted close to the bottom of the flasks. All the experiments were run in duplicates.

2.3. Sample preparation and analysis

2.3.1. Transformation process monitoring

Samples with 1-mL aliquots were withdrawn and transferred to 1.5 mL centrifuge tubes periodically at 3, 25, 40, 60, and 90 h during the incubation and filtered with 0.22 μm membrane filters. Then, 20 μL of the aliquot suspensions were diluted to 10 mL with deionized distilled water and the absorbance spectra were measured at 600 nm on a V600 UV–vis spectrophotometer (Japan Spectroscopic Co., Ltd.). Additional 50 μL of the aliquot suspensions were diluted to 20 mL and the concentrations of dissolved organic carbon (DOC) were measured by a TOC-V CSH analyzer (Shimadzu, Japan). E600 was used to quantify the degrees of humification and its values were calculated as

follows:

$$E600\,(Lg^{-1}cm^{-1}) = A600 / DOC\,(g\,L^{-1}) \times L\,(cm) \quad (2)$$

where A600 and L are the absorbance at 600 nm and the length of the light path (1 cm in our research), respectively.

In addition, 2 mL aliquots of the reaction mixtures were periodically withdrawn and transferred to 50 mL centrifuge tubes. Then, the samples were acidified to pH 1 with concentrated HCl (1 M), equilibrated for 24 h, and centrifuged at 25,000 rpm for 30 min to separate the precipitates of HA from the solution containing FA and others. Next, the precipitated HA was washed with deionized water by centrifugation for three times and re-dissolved in 0.1 M NaOH. The FA-containing supernatants were passed through a mini column with XAD-8 resin to adsorb FA, and the resin was washed with ultrapure water until the effluent was colorless. Then, 0.1 M NaOH (30 mL) was added into the mini column and the effluent was collected. The HA and FA collections were adjusted to pH 7 prior to the DOC analysis. The extracted HA and FA were then vacuum freeze-dried and used for FTIR analysis.

The effective particle sizes were measured with dynamic light scattering (DLS) on NanoBrook-Omni (Brookhaven) to probe the formation process of HA. NaCl (0.04%) was added prior to conducting DLS measurements. Each HA sample solution (5 mL, pH 7.0) was kept inside a cuvette and sealed with a plastic cap in the instrument for 120 s to reach an equilibrium temperature of 25 °C before starting the laser at a scattering angle of 90° with three replicates. Data on the HA particle sizes was collected in the intensity PSD mode. The autocorrelation function was used to treat the suspension's light intensity signals for the average effective diameter [34].

2.3.2. Characterization of the MnO_2 before and after the reactions

At the end of 90-h reaction, the solid residues were repeatedly washed with ultrapure distilled water by centrifugation at 20,000*g* for 20 min until the washed water was clear and finally dried at 80 °C for further structural analyses by XPS.

2.4. Analytical

2.4.1. FTIR spectroscopy

The freeze-dried HA and FA samples (10 mg each) were mixed with 150 mg predried-pulverized spectroscopic-grade KBr, ground and pressed under the irradiation of an infrared lamp to eliminate moisture in the samples. The absorbance spectra were recorded in the 4000–400 cm^{-1} range on a Perkin–Elmer 16F PC FTIR pectrophotometer, and each spectrum was obtained after 32 scans with 4 cm^{-1} resolution. The obtained FTIR spectra were smoothed and baseline corrected.

2.4.2. XPS analyses

The surface elemental contents of MnO_2 before (Fig. S2) and after the reactions were obtained by X-ray photoelectron spectroscopy (XPS, Thermo Fisher ESCALB 250X) in an ion-pumped chamber of an Escalad5 spectrometer [35].

2.5. 2D-COS analysis

2D-COS can provide additional structural change information compared with the conventional one dimensional spectra, by extending the spectra along the second dimension of the intensity change. This can discern the relative direction as well as the sequential order of structural variations. 2D-COS has been recently successfully expanded to probe the mechanisms of physiochemical processes in the environment, such as the adsorption mechanism of HA at the molecular level by examining the sequential order of the corresponding functional groups adsorbed [36–40]. To obtain the characteristics of FA/HA evolution in terms of the functional groups, 2D-COS coupled with FTIR spectra with incubation time as the external perturbation was employed in our research. The correlation peaks appeared on the synchronous and asynchronous spectra can be well interpreted by a set of established principles [41]. Briefly, the synchronous spectra consist of auto-peaks located along the main diagonal and cross-peaks located symmetrically at the off-diagonal positions of the map. In the synchronous map, the susceptibility of spectral intensity changes generates positively correlated auto-peaks, while the coordinated changes of spectral intensities observed at two different spectral variables indicate cross-peaks. A positive cross-peak sign indicates that the two spectral intensities change in the same direction, while a negative value indicates the opposite. The asynchronous spectra are based on the cross-correlation of the synchronous spectra and show cross-peaks exclusively. The signs represent the dynamics of spectral intensity variations with the sequential or out-of-phase changes induced by the perturbation. The two correlation spectra should be combined to decide the direction of spectral intensity variations and the sequential order of the perturbation. The details of the decision method are outlined by Noda and Ozaki [36–38,42]. For example, if the signs of the spectral coordinates (x_1, x_2) are the same in both the synchronous and asynchronous maps, the spectral intensity change at x_1 occurs predominantly prior to that at x_2. This order is reversed when the signs are opposite. In addition, if there is only synchronous correlation intensity, the spectral changes occur simultaneously, and if there is only asynchronous correlation intensity, the temporal relationship of the spectral intensity changes cannot be determined. The correlation maps were calculated using 2D Shige that was created by the Kwansei-Gakuin University. The Origin 2019b software was employed to plot all the maps.

3. Results and discussion

3.1. The degree of humification

When using the extinction coefficient (E600) as the indicator for the extent of humification (Fig. 1), the values of E600 in N_2 in the absence of MnO_2 remained almost zero throughout the 90-h incubation period, indicating that all the processes observed in the four reaction systems were abiotic. E600 in MnO_2 (N_2) only slightly increased, suggesting that MnO_2 itself exhibited a weak oxidization ability to promote the

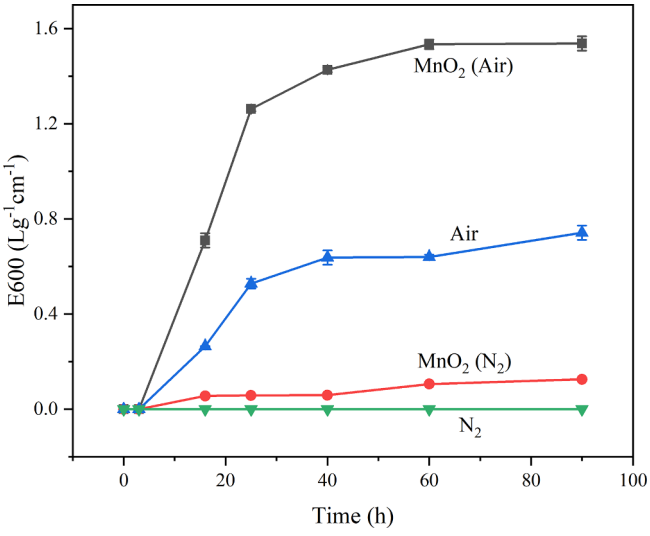

Fig. 1. Time courses of E600 in the four reaction systems during the 90-h reaction period. Reaction conditions: catechin 0.008 M, glycine 0.02 M, initial pH 8.0, in the presence or absence of 2 g of MnO_2 under ambient O_2 (Air) or N_2 (N_2) conditions at 45 °C. The reaction conditions were the same for all the figures below. Symbols and bars represent the mean values and standard deviations of duplicate measurements (some error bars are obscured by the symbols).

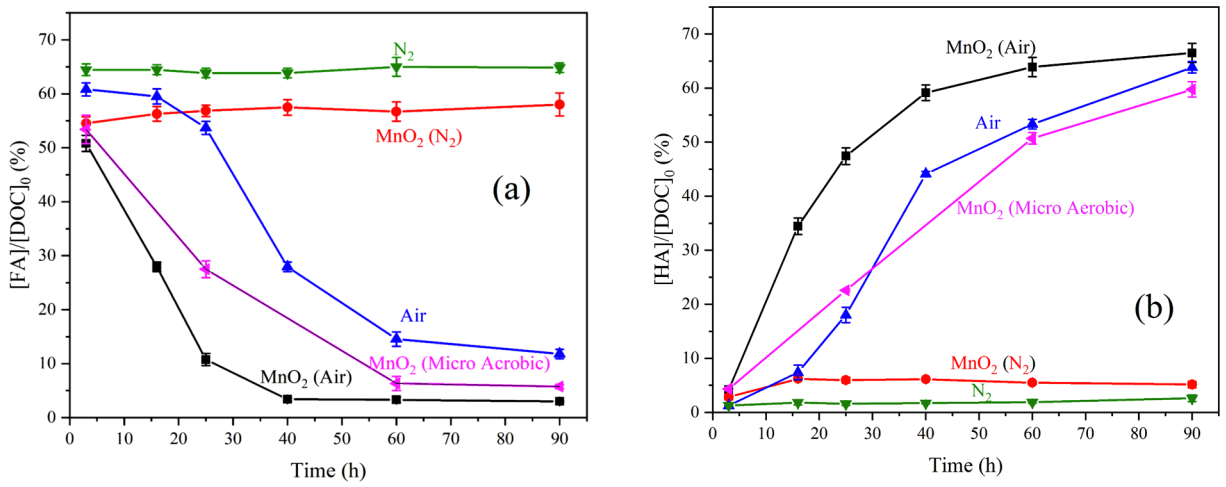

Fig. 2. Effects of MnO_2 and O_2 in the four reaction systems on the formation of FA (a) and HA (b) at 45 °C during the 90-h reaction period. The data points are given as means with standard deviations. The fifth system "MnO_2 (Micro Aerobic)" is the system containing MnO_2 and a small amount of air (a typical experimental setup in the bulk of the literature).

humification. In contrast, E600 in MnO_2 (Air) significantly increased in the first 24 h and reached plateau after 60 h, while E600 in Air followed a similar trend but at lower values. The above results proved that O_2 played a key role in the abiotic humification process and MnO_2 mainly acted as a catalyst to enhance the amount of HS produced. This finding agrees well with previous research showing that there was a synergistic effect of MnO_2 and O_2 in promoting the conversion of simple phenolic compounds to HS [10,23].

3.2. The kinetics of HS production in the four reaction systems

In order to understand the evolution of HA and FA during the abiotic humification process, HS was extracted from the supernatants at different incubation times and the DOC concentrations of the extracted FA and HA were analyzed. The fractions (%) of FA and HA in the four systems during the reaction period are shown in Fig. 2. As shown in Fig. 2a, FA formed quickly within < 3 h, remained stable during the 90-h reaction, and accounted for approximately 65% and 55% of the DOC in the systems of N_2 and MnO_2 (N_2), respectively. With the additional ~5% of HA formed in MnO_2 (N_2) (Fig. 2b), there was approximately 5% difference in the total DOC of the extracted humic substances between the two reaction systems. This may be related to the adsorption of the formed humic substances on the surface of MnO_2 that could not be entirely recovered during the acid/base extraction. A similar difference was also obtained between the systems of Air and MnO_2 (Air) (Fig. 2). Moreover, the fractions of FA formed in the systems of MnO_2 (Air) and Air were comparable initially but decreased quickly with time. Note that FA is an intermediate in the process of humification [21,31]; thus, it is likely that FA had transformed into HA in the two systems containing oxygen to result in the decrease in its concentration. It also seems that MnO_2 in the absence of O_2 was unable to transform FA into HA, which might be ascribed its low oxidizing capability at pH > 7, as explained below.

As for the fraction of HA, it was almost negligible in N_2 and remained low in MnO_2 (N_2) (Fig. 2b), indicating that the formation of HA was not a result of the direct oxidation by MnO_2. In fact, the direct oxidative reactivity of MnO_2 was highly pH dependent and decreased significantly with increasing pH [43,44]. The pH values in our reaction systems decreased from 8 to around neutral (Fig. S3); therefore, the direct oxidative reactivity of MnO_2 only played a minor role in the total oxidative reactivity. On the contrary, the fraction of HA (commonly used to describe HS production) generated in the system of MnO_2 (Air) showed a rapid growth within the first 20 h and then gradually increased until reaching a plateau. The trend in Air was similar, with an almost similar amount of HA produced at 90 h but at a slower HA production rate in the first half of the reaction. For comparison, we conducted an additional experiment to examine the FA and HA formation with MnO_2 but with a small amount of O_2 introduced during the reaction period (a typical practice in most of the research in the field). It turns out that the FA/HA formation kinetics were between those of MnO_2 (N_2) and MnO_2 (Air) (Fig. 2a, b).

Based on these findings, we confirmed that (1) molecular O_2 played a dominant role in the formation of HA from FA, which is similar to the results obtained above using E600 as the indicator; (2) FA can form under slightly alkaline conditions without O_2 or MnO_2; and (3) MnO_2 did not affect the conversion of FA to HA because of its limited oxidative ability under the given conditions. As suggested by the results from the previous research on abiotic humification with MnO_2 in the presence of a small amount of O_2, MnO_2 mediated the formation of FA, which in turn affected the production of HA [21,31]. Therefore, similar to many other applications [5,45,46], MnO_2 should mainly work as a catalyst rather than a direct oxidant during the humification process.

3.3. The evolution of HA size

Dynamic light scattering (DLS) is a useful method for investigating particle sizes and can reflect the molecular weight in some cases [47]. Numerous studies have reported that environmental occurring HAs have a wide range of sizes (40 nm to several micrometers) [40,48,49], which would influence the colloidal stability and functions in nature [49]. The average effective diameter of the final humification product (i.e., HA) in this work was measured by the DLS method, and the kinetic date was fitted using the sigmoidal function with a logistic model:

$$y = a/(1 + exp(-k\times(t-t_c)) \quad (3)$$

where y is the effective diameter (nm) at a given incubation time t (h); k is the slope of the curve; a denotes the maximum effective diameter of the reaction product (nm); and t_c (h) is the time when the effective diameter has the greatest change.

As shown in Fig. 3, the effective diameter of HA in Air only slightly increased and that in N_2 remained very small. In contract, it gradually but significantly increased with time in both MnO_2 (Air) and MnO_2 (N_2), indicating that MnO_2 played a vital role in promoting the increase in the HA size. The size of HA in MnO_2 (N_2) was however very small until about 40 h (Fig. 3 inset) and then increased rapidly at around 56.9 h (Table 1). According to some related research on the characteristics of humic acids [50–52], this might have been due to the low concentration of HA formed in the initial stage (Fig. 2b), and a longer

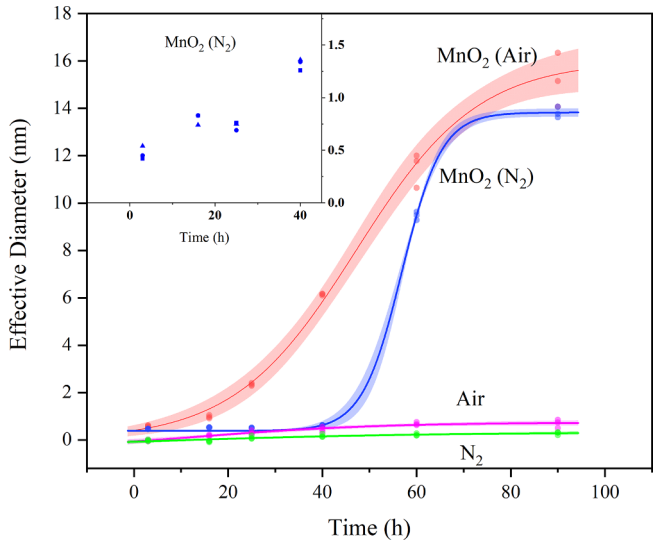

Fig. 3. Time course of the effective diameter of HA in the four reaction systems. The lines were the fitting based on Eq. (3) with 95% confidence levels. Inset: time course of the effective diameter of HA in MnO_2 (N_2) in the first 40 h.

Table 1
Model fitting parameters for the formation of HA in the four systems.

System	k (h^{-1})	a (nm)	t_c (h)	r^2
MnO_2 (Air)	0.175	16.0	47.2	0.9869
MnO_2 (N_2)	0.237	13.8	56.9	0.9994
Air	0.0509	0.651	13.7	0.9046
N_2	0.0329	0.0425	1.39	0.7794

period was needed for a sufficient amount of small sized HA to accumulate on the surface of MnO_2. Afterwards, the size would grow more quickly due to hydrogen bonding and/or intermolecular hydrophobic forces [50]. This may be the reason that the rapid increase in the HA size occurred at around 56.9 h in MnO_2 (N_2). Nevertheless, we can still conclude that the size of HA formed in the abiotic process was mostly determined by the presence of MnO_2. This result for the first time confirmed the hypothesis in earlier studies [12,15] that MnO_2 had a contribution to the formation of HS with higher aromaticity.

3.4. Effects of oxygen and MnO_2 on the evolution of HS functional groups

FTIR analysis has served as a useful qualitative tool to identify the functional groups of HS [3,6]. The one-dimensional FTIR spectra of HA in the MnO_2 (Air) reaction system in the 3500–800 cm^{-1} region are illustrated in Fig. 4a as an example. The absorption intensities of the peaks at 3450, 1590, 1380, and 1080 cm^{-1} were sensitive to the reaction time. As shown in Fig. 4b, the absorption intensity of all four peaks increased with incubation time. However, the spectroscopic observations were not sufficiently sensitive to reveal the dynamics in the structure evolution of HA. Also, the absorption spectra strongly overlapped in the region of 1750–800 cm^{-1}. Therefore, one-dimensional FTIR spectra were not able to provide detailed information on the evolution of HA characteristics, with the strongly overlapped absorption peaks caused by the diverse groups of HA.

To further probe the transformation sequence of HS functional groups over time, 2D-COS analysis was performed. The results of the evolution of FA and HA molecular structures in the four reaction systems are displayed in Figs. 5 and 6, and the detailed peak assignments and signs of each cross-peak in the synchronous and asynchronous maps of FA and HA in the four systems are summarized in Tables S1–S8.

Comparing the synchronous maps for the four reaction systems (Fig. 5S), the accumulation of the functional groups of FA was most significant in MnO_2 (N_2) (Fig. 5b), less significant in N_2 (Fig. 5d), and much less obvious in MnO_2 (Air) and Air (Fig. 5a and c). Therefore, it is likely that FA, an intermediate product, was quickly transformed to HA in the presence of oxygen. Here, we use the system of MnO_2 (N_2) as an example to explain the evolution of the FA functional groups. Almost all cross-peaks in the synchronous map of MnO_2 (N_2) were positive (Fig. 5b and Table S2), indicating that the changes are in the same direction. Specifically, there are six predominant auto-peaks on the diagonal line at 3450, 3250, 1590, 1450, 1380 and 1220 cm^{-1}, with the peak at 3450 cm^{-1} the most significant (Fig. 5b). The band at around 3450 cm^{-1} is likely due to hydrogen bonds [53–56]. Moreover, majority of the auto-peaks on the asynchronous maps exhibited negative signs with some positive signs, suggesting that while FA continued to form, there might be some FA transformed into other components such as HA (Fig. 5f, Table S2). Therefore, we can conclude that the structure changes of FA were dynamic, which further confirmed that FA was an intermediate.

The evolution pattern of HA in MnO_2 (Air) (Fig. 6a) is much stronger than that in the other systems (Fig. 6S). The evolution pattern of HA in Air (Fig. 6c) was similar but less significant. The pattern in MnO_2 (N_2) was weak (Fig. 6b) and there was barely any signal in N_2 (Fig. 6d), agreeing with the small to negligible amounts of HA formed in the two systems (Figs. 1 and 2b), despite the large HA diameters observed in MnO_2 (N_2) (Fig. 3). These results demonstrated that O_2 had the dominant effect on the progressive formation of the HA function groups.

Because of the strongest signals, the results in MnO_2 (Air) were selected as a representative model to analyze the functional group evolution of HA. Specifically, there are eight predominant auto-peaks on the diagonal line (Fig. 6a), with the detailed peak assignments and signs in Table S5. Based on the Noda's rule, we can see that the eight cross-peaks have positive signs in the synchronous map, suggesting the same intensity changes of these peaks. When combining with the negative corresponding cross-peaks in the asynchronous maps (Fig. 6e and Table S5), we can conclude that the structural change of HA functional groups followed the order of 1220cm^{-1} > 1380cm^{-1} > 1450cm^{-1}~1080cm^{-1} > 1590cm^{-1} > 1730-cm^{-1} > 3250 cm^{-1} > 3450 cm^{-1}, corresponding to stretching of the C–OH bond in carboxylic acids [42] > C–OH stretching in phenolic OH [38,40] > aromatic C—C bands ~C—O carbohydrates, aromatic ether [39] > amide and carboxylate C═O [42,56] > COO^- symmetric stretching [41] > NH stretching [56] > hydrogen bond [57]. These results show that the COO^- symmetric stretching appeared after aromatic C—C, suggesting that the carboxylate groups had developed as a result of ring cleavage of the polyphenol in the presence of O_2, which directly confirmed the important role of O_2 in promoting the degradation of phenolic compounds [14,15,23,58]. Moreover, the peak at 3450 cm^{-1} appeared in the reaction systems of MnO_2 (Air) and MnO_2 (N_2), suggesting that hydrogen bonding might be involved in the formation of HA, although further research is needed to confirm this observation. The reason for less significant auto-peaks in MnO_2 (N_2) (Fig. 6b) than in MnO_2 (Air) was that there was only limited oxidation by MnO_2 that resulted in a small quantity of HA.

3.5. Characterization of MnO_2 before and after reaction with XPS

From the above analysis, we have already identified the role of MnO_2 in the abiotic formation of humic substances. XPS analysis was further used to obtain the surface Mn oxidation states as a supplemental material to support the role of MnO_2. The method used in this work for fitting various Mn oxidation states followed the work in the Handbook of the Elements and Native Oxides, which is deemed to be reliable by XPS international, Inc. [59].

As shown in Fig. 7b, Mn 2p3/2 from the MnO_2 residue in MnO_2 (N_2) can be best matched with three peaks. The peaks with the binding energies of 640.7 [60], 641 and 641.6 eV [61] correspond to Mn(II), Mn

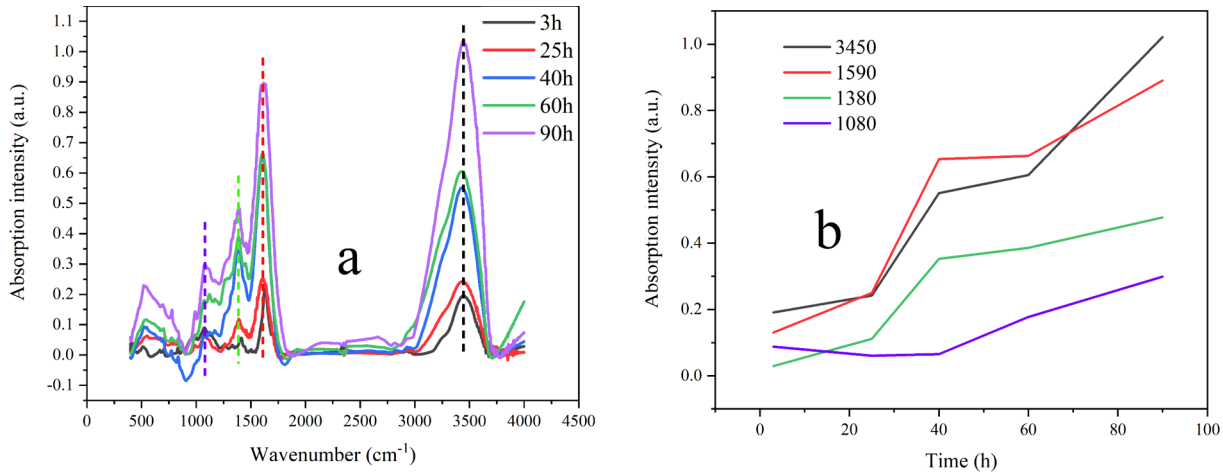

Fig. 4. (a) The FTIR spectra of HA in the reaction system of MnO_2 (Air) at different reaction times. (b) The intensity changes of four peaks (3450, 1590, 1380and 1080 cm^{-1}) over time that were extracted from (a).

(III) and Mn(IV) with the intensity of 4.1%, 15.1% and 80.9%, respectively. Compared with the original MnO_2 XPS spectrum with > 99% as Mn(IV) (Fig. S1), the abundance of Mn(III) increased and that of Mn(IV) decreased, indicating that MnO_2 was reduced in oxidizing the catechin-glycine mixture. However, there are only two peaks at 641 and 641.6 eV in MnO_2 (Air), indicating the existence of only Mn(III) (10%) and Mn(IV) (90%) on the surface of MnO_2. Compared with the MnO_2 residue under N_2, the Mn(III) content in MnO_2 (Air) decreased, while that of Mn(IV) increased. Note that we also followed other reported fitting parameters [60,61] with the binding energies of 640.8, 641.4 and 641.9 eV for Mn(II), Mn(III) and Mn(IV), respectively, and obtained similar changes in the Mn(III) and Mn(IV) contents in the MnO_2 residues after the reaction (data not shown). Previous studies have shown that when MnO_2 acted as direct oxidants, the Mn(III) content increased and that of Mn(IV) decreased [62]; however, when MnO_2 acted as catalysts, the Mn(III) content decreased and that of Mn(IV) increased [5,26]. Therefore, the difference between these two MnO_2 residues resulted mostly from the catalytic reactivity and only slightly from the oxidative reactivity. This finding is similar to previous studies [25,26] and the discussion above (Sections 3.1 and 3.2). Moreover, the less Mn (III) content in MnO_2 (Air) could be partly ascribed to its oxidation by O_2. However, future research is warranted to understand more details of the decrease in the Mn(III) content and how MnO_2 was engaged in the reaction.

4. Conclusions

This work detailed the specific roles of O_2 and MnO_2 in their synergistic effects on the formation of HS during the humification process. MnO_2 alone had a weak oxidative ability in promoting the

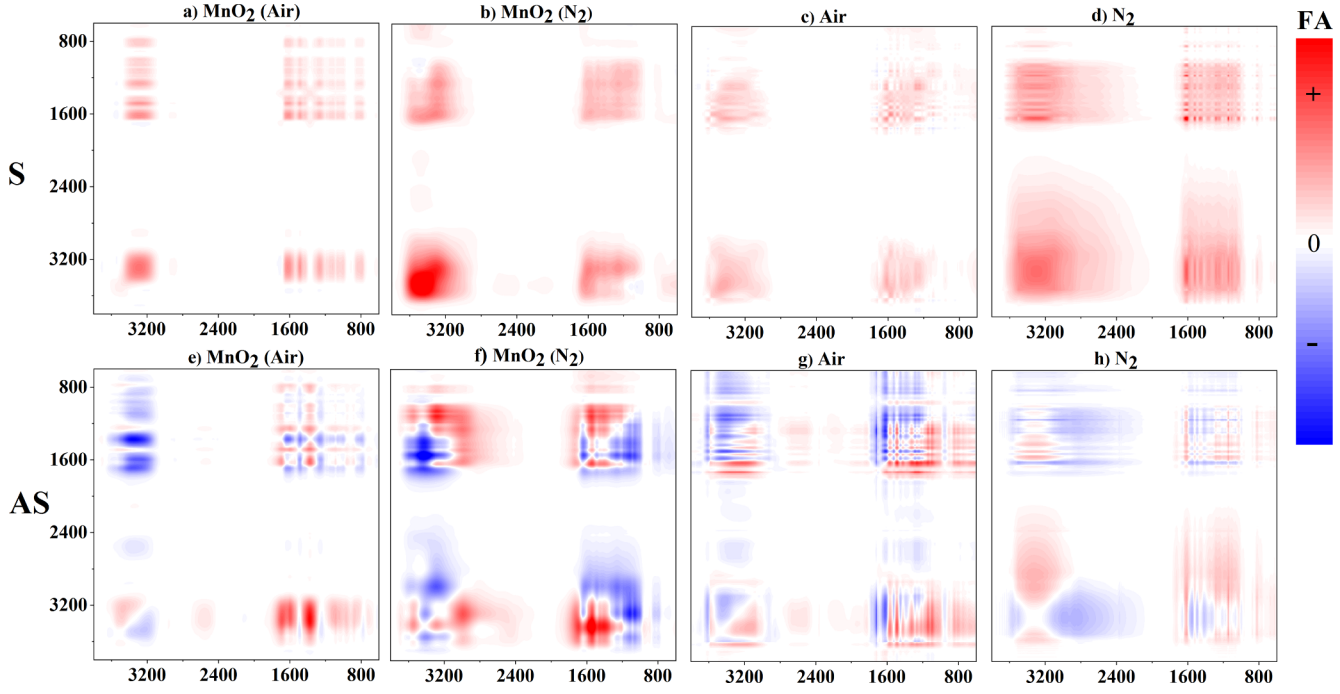

Fig. 5. Synchronous (S) and asynchronous (AS) 2D correlation maps with incubation time as the perturbation were generated from the FTIR spectra of FA in the four reaction systems at 3, 16, 26, 40, 60, and 90 h in the 4000–600 cm^{-1} region. The color changing from blue to red illustrates the change in the correlation intensity from negative to positive (similar for Fig. 6). (For interpretation of the references to color in this figure legend, the reader is referred to the web version of this article.)

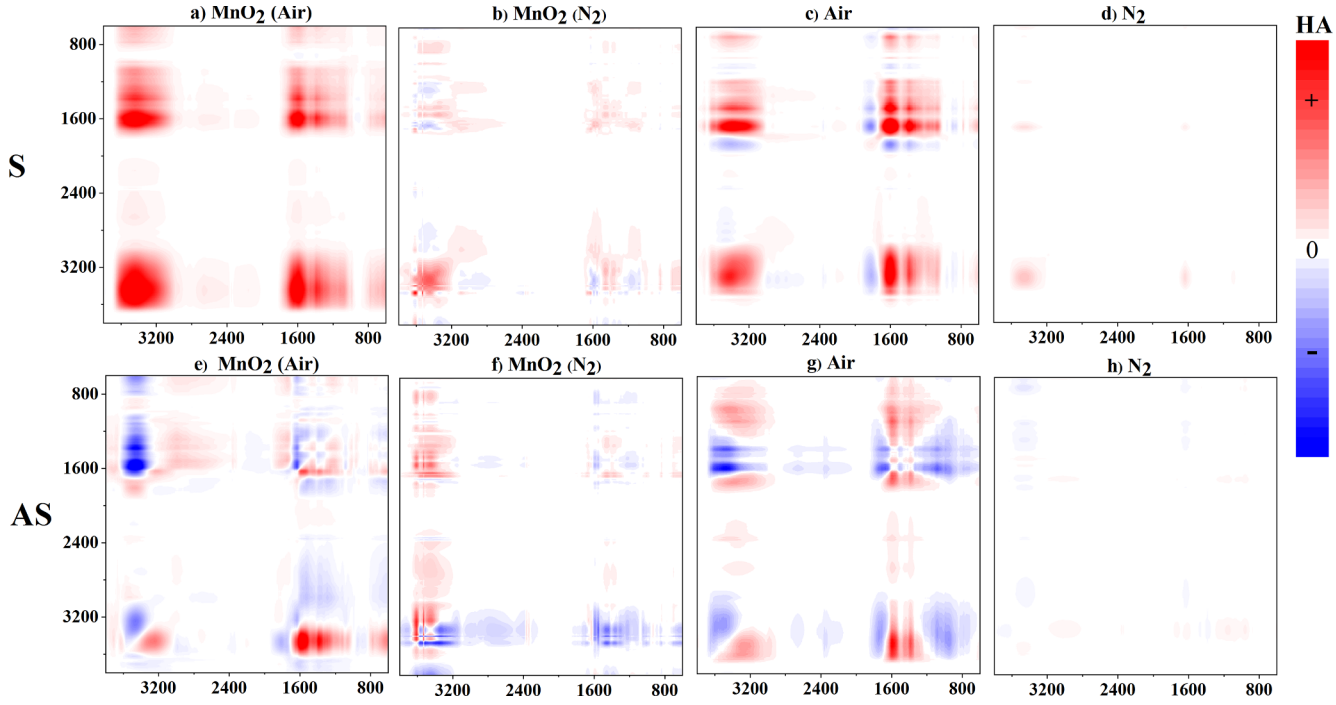

Fig. 6. Synchronous (S) and asynchronous (AS) 2D correlation maps with the incubation time as the perturbation were generated from the FTIR spectra of HA in the four reaction systems at 3, 16, 26, 40, 60, and 90 h in the 4000–600 cm^{-1} region.

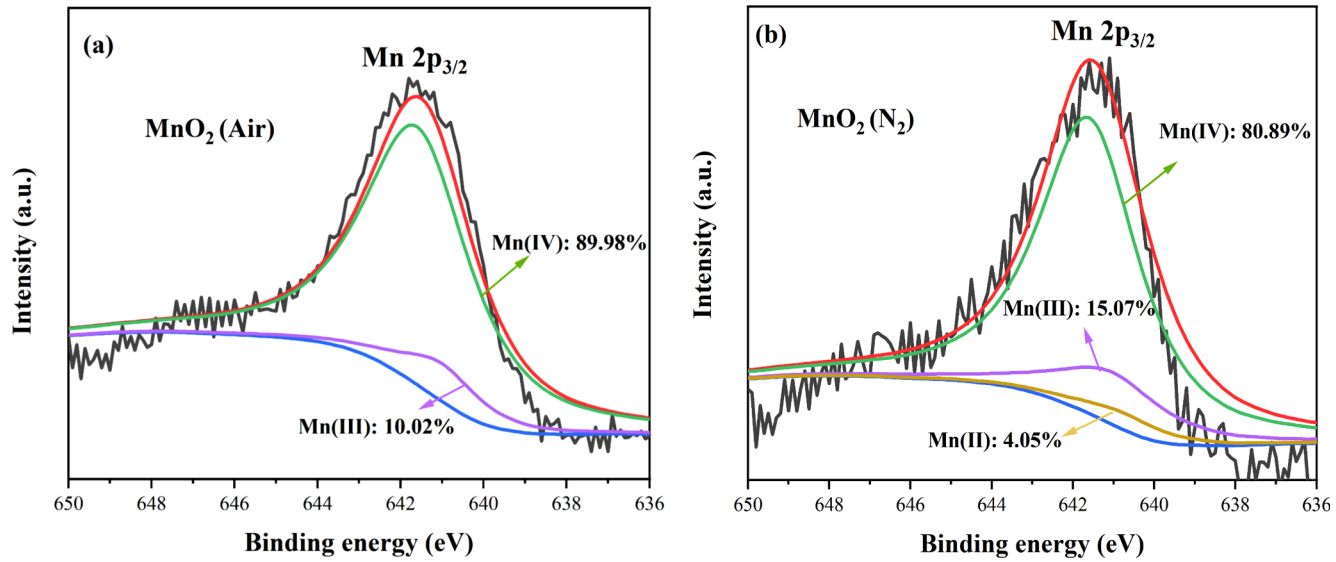

Fig. 7. XPS spectra of Mn $2p_{3/2}$ of MnO_2 residue in the catechin-glycine reaction systems under a) Air and b) N_2.

humification, whereas O_2 was indispensable in the HA formation and largely determined the amount of HA formed. In the presence of O_2, however, MnO_2 significantly enhanced both the extent of abiotic humfication and the size of the formed HA. To the best of the authors' knowledge, this is the first report on the individual roles of MnO_2 and O_2 in the humification process in model systems, which provided a valuable addition to the theory of abiotic humification and will facilitate the development of treatment technologies for bio-wastes. Future research will focus on how MnO_2 facilitates the HA formation and what properties of MnO_2 influence the process. This information will enable better understanding of natural humification processes and allow the synthesis of new catalysts that can more cost-efficiently produce stable HS.

Declaration of Competing Interest

The authors declare that they have no known competing financial interests or personal relationships that could have appeared to influence the work reported in this paper.

Acknowledgments

This manuscript is based on work support from National Key R&D Program of China, No. 2018YFC1901405. The authors are grateful to Shigeaki Morita in Professor Yukihiro Ozaki's group at the Kwansei-Gakuin University for providing the 2Dshige software. H. Zhang acknowledges the support from the U. S. National Science Foundation

through Grant # CHE-1808406.

Appendix A. Supplementary data

Supplementary data to this article can be found online at https://doi.org/10.1016/j.cej.2020.124734.

References

[1] F.J. Stevenson, Humus chemistry: genesis, composition, reactions, John Wiley & Sons1994.
[2] L. Zhang, X. Sun, Changes in physical, chemical, and microbiological properties during the two-stage co-composting of green waste with spent mushroom compost and biochar, Bioresour. Technol. 171 (2014) 274–284.
[3] C. Wang, Q. Tu, D. Dong, P.J. Strong, H. Wang, B. Sun, W. Wu, Spectroscopic evidence for biochar amendment promoting humic acid synthesis and intensifying humification during composting, J. Hazard. Mater. 280 (2014) 409–416.
[4] Z. Zhang, Y. Zhao, R. Wang, Q. Lu, J. Wu, D. Zhang, Z. Nie, Z. Wei, Effect of the addition of exogenous precursors on humic substance formation during composting, Waste Manage. 79 (2018) 462–471.
[5] J. Huang, Y. Dai, K. Singewald, C. Liu, S. Saxena, H. Zhang, Effects of MnO_2 of different structures on activation of peroxymonosulfate for bisphenol A degradation under acidic conditions, Chem. Eng. J. 370 (2019) 906–915.
[6] S. Amir, A. Jouraiphy, A. Meddich, M. El Gharous, P. Winterton, M. Hafidi, Structural study of humic acids during composting of activated sludge-green waste: elemental analysis, FTIR and ^{13}C NMR, J. Hazard. Mater. 177 (2010) 524–529.
[7] K. Jindo, T. Sonoki, K. Matsumoto, L. Canellas, A. Roig, M.A. Sanchez-Monedero, Influence of biochar addition on the humic substances of composting manures, Waste Manage. 49 (2016) 545–552.
[8] M.E. Silva, L.T. de Lemos, O.C. Nunes, A.C. Cunha-Queda, Influence of the composition of the initial mixtures on the chemical composition, physicochemical properties and humic-like substances content of composts, Waste Manage. 34 (2014) 21–27.
[9] H. Qi, Z. Wei, J. Zhang, Y. Zhao, J. Wu, X. Gao, Z. Liu, Y. Li, Effect of MnO_2 on biotic and abiotic pathways of humic-like substance formation during composting of different raw materials, Waste Manage. 87 (2019) 326–334.
[10] H. Shindo, P. Huang, Role of Mn(IV) oxide in abiotic formation of humic substances in the environment, Nature 298 (1982) 363–365.
[11] H. Shindo, P. Huang, Significance of Mn(IV) oxide in abiotic formation of organic nitrogen complexes in natural environments, Nature 308 (1984) 57–58.
[12] M. Wang, P. Huang, Characteristics of pyrogallol-derived polymers formed by catalysis of oxides, Soil Sci. 165 (2000) 737–747.
[13] A.G. Hardie, J.J. Dynes, L.M. Kozak, P. Huang, Abiotic catalysis of the maillard and polyphenol-maillard humification pathways by soil clays from temperate and tropical environments, 2010.
[14] A. Jokic, M.C. Wang, C. Liu, A.I. Frenkel, P. Huang, Integration of the polyphenol and Maillard reactions into a unified abiotic pathway for humification in nature: the role of delta-$MnO_{(2)}$, Org. Geochem. 35 (2004) 747–762.
[15] M. Wang, P. Huang, Ring cleavage and oxidative transformation of pyrogallol catalyzed by Mn Fe, Al, and Si oxides, Soil Sci. 165 (2000) 934–942.
[16] M. Wang, P. Huang, Cleavage and polycondensation of pyrogallol and glycine catalyzed by natural soil clays, Geoderma 112 (2003) 31–50.
[17] J. Gao, C. Hedman, C. Liu, T. Guo, J.A. Pedersen, Transformation of sulfamethazine by manganese oxide in aqueous solution, Environ. Sci. Technol. 46 (2012) 2642–2651.
[18] M. Ahn, C. Martinez, D. Archibald, A. Zimmerman, J. Bollag, J. Dec, Transformation of catechol in the presence of a laccase and birnessite, Soil Biol. Biochem. 38 (2006) 1015–1020.
[19] A. Jokic, A.I. Frenkel, P. Huang, Effect of light on birnessite catalysis of the Maillard reaction and its implication in humification, Can. J. Soil Sci. 81 (2001) 277–283.
[20] A. Jokic, A.I. Frenkel, M.A. Vairavamurthy, P. Huang, Birnessite catalysis of the Maillard reaction: Its significance in natural humification, Geophys. Res. Lett. 28 (2001) 3899–3902.
[21] Y. Zhang, D. Yue, X. Wang, W. Song, Mechanism of oxidation and catalysis of organic matter abiotic humification in the presence of MnO_2, J. Environ. Sci. 77 (2019) 167–173.
[22] Y. Zhang, D. Yue, X. Lu, K. Zhao, H. Ma, Role of ferric oxide in abiotic humification enhancement of organic matter, J. Mater. Cycles Waste. 19 (2017) 585–591.
[23] C. Chien, H. Chen, M. Wang, K. Seshaiah, Oxidative degradation and associated mineralization of catechol, hydroquinone and resorcinol catalyzed by birnessite, Chemosphere 74 (2009) 1125–1133.
[24] S. Zhu, S.H. Ho, C. Jin, X. Duan, S. Wang, Nanostructured manganese oxides: natural/artificial formation and their induced catalysis for wastewater remediation, Environ. Sci. Nano. 7 (2019) 368–396.
[25] J. Huang, H. Zhang, Mn-based catalysts for sulfate radical-based advanced oxidation processes: a review, Environ. Int. 133 (2019) 105–141.
[26] J. Huang, H. Zhang, Oxidant or catalyst for oxidation? The role of manganese oxides in the activation of peroxymonosulfate (PMS), Front. Environ. Sci. Eng. 13 (2019) 65.
[27] B.N. Singh, S. Shankar, R.K. Srivastava, Green tea catechin, epigallocatechin-3-gallate (EGCG): mechanisms, perspectives and clinical applications, Biochem. Pharmacol. 82 (2011) 1807–1821.
[28] G. Qi, D. Yue, M. Fukushima, S. Fukuchi, R. Nishimoto, Y. Nie, Enhanced humification by carbonated basic oxygen furnace steel slag–II. Process characterization and the role of inorganic components in the formation of humic-like substances, Bioresour. Technol. 114 (2012) 637–643.
[29] G. Qi, D. Yue, M. Fukushima, S. Fukuchi, Y. Nie, Enhanced humification by carbonated basic oxygen furnace steel slag - I. Characterization of humic-like acids produced from humic precursors, Bioresour. Technol. 104 (2012) 497–502.
[30] J. Huang, S. Zhong, Y. Dai, C.C. Liu, H. Zhang, Effect of MnO_2 phase structure on the oxidative reactivity toward bisphenol a degradation, Environ. Sci. Technol. 52 (2018) 11309–11318.
[31] Y. Zhang, D. Yue, H. Ma, Darkening mechanism and kinetics of humification process in catechol-Maillard system, Chemosphere 130 (2015) 40–45.
[32] A.G. Hardie, J.J. Dynes, L.M. Kozak, P. Huang, The role of glucose in abiotic humification pathways as catalyzed by birnessite, J. Mol. Catal. A Chem. 308 (2009) 114–126.
[33] A.G. Hardie, J.J. Dynes, L.M. Kozak, P. Huang, Biomolecule-induced carbonate genesis in abiotic formation of humic substances in nature, Can. J. Soil Sci. 89 (2009) 445–453.
[34] M.R. Esfahani, H.A. Stretz, M.J. Wells, Abiotic reversible self-assembly of fulvic and humic acid aggregates in low electrolytic conductivity solutions by dynamic light scattering and zeta potential investigation, Sci. Total Environ. 537 (2015) 81–92.
[35] J. Zhang, J. Chen, Q. Zhang, R. Wang, S. Wu, One step synthesis of one dimensional nano MnO_2 and their application as oxidizing agent for polysulfide polymers, J. Inorg. Organomet. P 29 (2019) 1400–1406.
[36] W. Chen, C. Teng, C. Qian, H. Yu, Characterizing properties and environmental behaviors of dissolved organic matter using two-dimensional correlation spectroscopic analysis, Environ. Sci. Technol. 53 (2019) 4683–4694.
[37] W. Chen, C. Qian, X. Liu, H. Yu, Two-dimensional correlation spectroscopic analysis on the interaction between humic acids and TiO2 nanoparticles, Environ. Sci. Technol. 48 (2014) 11119–11126.
[38] W. Chen, N. Habibul, X. Liu, G. Sheng, H. Yu, FTIR and synchronous fluorescence heterospectral two-dimensional correlation analyses on the binding characteristics of copper onto dissolved organic matter, Environ. Sci. Technol. 49 (2015) 2052–2058.
[39] B.M. Lee, J. Hur, Adsorption behavior of extracellular polymeric substances on graphene materials explored by fluorescence spectroscopy and two-dimensional fourier transform infrared correlation spectroscopy, Environ. Sci. Technol. 50 (2016) 7364–7372.
[40] Y. Yuan, X. Cai, B. Tan, S. Zhou, B. Xing, Molecular insights into reversible redox sites in solid-phase humic substances as examined by electrochemical in situ FTIR and two-dimensional correlation spectroscopy, Chem. Geol. 494 (2018) 136–143.
[41] I. Noda, Y. Ozaki, Two-Dimensional Correlation Spectroscopy: Applications in Vibrational and Optical Spectroscopy, John Wiley & Sons, 2005.
[42] W. Chen, Z. Ouyang, C. Qian, H. Yu, Induced structural changes of humic acid by exposure of polystyrene microplastics: a spectroscopic insight, Environ. Pollut. 233 (2018) 1–7.
[43] H. Zhang, W. Chen, C. Huang, Kinetic modeling of oxidation of antibacterial agents by manganese oxide, Environ. Sci. Technol. 42 (2008) 5548–5554.
[44] A.T. Stone, Reductive dissolution of manganese(III/IV) oxides by substituted phenols, Environ. Sci. Technol. 21 (1987) 979–988.
[45] D.M. Robinson, Y.B. Go, M. Mui, G. Gardner, Z. Zhang, D. Mastrogiovanni, E. Garfunkel, J. Li, M. Greenblatt, G.C. Dismukes, Photochemical water oxidation by crystalline polymorphs of manganese oxides: structural requirements for catalysis, J. Am. Chem. Soc. 135 (2013) 3494–3501.
[46] Y. Meng, W. Song, H. Huang, Z. Ren, S. Chen, S.L. Suib, Structure-property relationship of bifunctional MnO_2 nanostructures: highly efficient, ultra-stable electrochemical water oxidation and oxygen reduction reaction catalysts identified in alkaline media, J. Am. Chem. Soc. 136 (2014) 11452–11464.
[47] S. Förster, M. Schmidt, M. Antonietti, Static and dynamic light scattering by aqueous polyelectrolyte solutions: effect of molecular weight, charge density and added salt, Polymer 31 (1990) 781–792.
[48] M. Klučáková, K. Věžníková, Micro-organization of humic acids in aqueous solutions, J. Mol. Struct. 1144 (2017) 33–40.
[49] M. Klucakova, Size and charge evaluation of standard humic and fulvic acids as crucial factors to determine their environmental behavior and impact, Front. Chem. 6 (2018).
[50] A. Piccolo, In memoriam Prof. F.J. Stevenson and the Question of humic substances in soil, Chem. Biol. Technol. Agric. 3 (2016) 23.
[51] A.J. Simpson, Determining the molecular weight, aggregation, structures and interactions of natural organic matter using diffusion ordered spectroscopy, Magn. Reson. Chem. 40 (2002) S72–S82.
[52] A.J. Simpson, W.L. Kingery, M. Spraul, E. Humpfer, P. Dvortsak, R. Kerssebaum, Separation of structural components in soil organic matter by diffusion ordered spectroscopy, Environ. Sci. Technol. 35 (2001) 4421–4425.
[53] F. Wang, M. Feve, T.M. Lam, J.P. Pascault, FTIR analysis of hydrogen bonding in amorphous linear aromatic polyurethanes. I. Influence of temperature, J. Polym. Sci. B Polym. Phys. 32 (1994) 1305–1313.
[54] B. Chefetz, F. Adani, P. Genevini, F. Tambone, Y. Hadar, Y. Chen, Humic-Acid transformation during composting of municipal solid waste, J. Environ. Qual. 27 (1998) 794–800.
[55] P. Castaldi, G. Alberti, R. Merella, P. Melis, Study of the organic matter evolution during municipal solid waste composting aimed at identifying suitable parameters for the evaluation of compost maturity, Waste Manage. 25 (2005) 209–213.
[56] C. Garcia, T. Hernandez, F. Costa, Comparison of humic acids derived from city refuse with more developed humic acids, Soil Sci. Plant Nutr. 38 (1992) 339–346.
[57] M. Mecozzi, E. Pietrantonio, M. Pietroletti, The roles of carbohydrates, proteins and lipids in the process of aggregation of natural marine organic matter investigated by

means of 2D correlation spectroscopy applied to infrared spectra, Spectrochim. Acta. Part A 71 (2009) 1877–1884.
[58] M. Wang, P. Huang, Cleavage of C-14-labeled glycine and its polycondensation with pyrogallol as catalyzed, Geoderma 124 (2005) 415–426.
[59] B.V. Crist, Handbook of the Elements and Native Oxides, XPS International Inc., Iowa, USA, 1999.
[60] H. Nesbitt, D. Banerjee, Interpretation of XPS Mn(2p) spectra of Mn oxyhydroxides and constraints on the mechanism of MnO_2 precipitation, Am. Mineral. 83 (1997) 305–315.
[61] C.N.R. Rao, D.D. Sarma, S. Vasudevan, M.S. Hegde, Study of transition metal oxides by photoelectron spectroscopy, Proc. R. Soc. London, Ser. A. 367 (1979) 239–252.
[62] N. Shaikh, S. Taujale, H. Zhang, K. Artyushkova, A.S. Ali, J.M. Cerrato, Spectroscopic investigation of interfacial interaction of manganese oxide with triclosan, aniline, and phenol, Environ. Sci. Technol. 50 (2016) 10978–10987.